Supporting Information

Ring Origami: Snap-folding of Rings with Different Geometries

Shuai Wu[§], Liang Yue[§], Yi Jin[§], Xiaohao Sun, Cole Zemelka, H. Jerry Qi, Ruike Zhao**

Supplementary Methods

1. Characterization of the polymer resin for ring fabrication

Standard tensile bars (ASTM D638) were prepared and tested using an MTS universal test machine (Model 41, MTS, Eden Prairie, USA) with a strain rate of 0.1 min^{-1}. Figure S2A shows the stress-strain curves of the cured resin under cyclic tensile tests up to at least 2% of strain, indicating a linear elastic behavior. Linear curve fitting of 1% strain indicates a Young's modulus of 1.8 GPa. Dynamic mechanical analysis (DMA) was conducted using DMA 850 (TA Instruments, USA) from 30°C to 200°C at a temperature rate of 10°C min^{-1}. The strain is oscillated at a frequency of 1 Hz with a peak-to-peak amplitude of 0.1%. Figure S2B shows the result of the DMA measurement, indicating a glass transition temperature of 118 °C.

2. Poisson's ratio's effect on snap-folding of circular rings

Plastics or metals such as stainless steel are usually considered as materials for ring fabrication. The material's Poisson's ratio (v) is within the range of 0.3~0.4. The results of two circular rings of materials with Young's modulus of 1.8 GPa and Poisson's ratio of 0.3 and 0.4 are compared to study the influence of Poisson's ratio on rings snap-folding. As shown in Figure S6, the folding behaviors are very similar for v=0.3 and 0.4, indicating a negligible effect of Poisson's ratio.

3. Calculation of the area ratio

The area ratio is defined by the following equation,

$$\eta = \frac{A_i}{A_f}, \tag{S1}$$

where A_i is the in-plane area of undeformed configuration, and A_f is the area of the deformed configuration by calculating the envelop area of its projection to the reference plane.

Supplementary Figures and Figure Captions

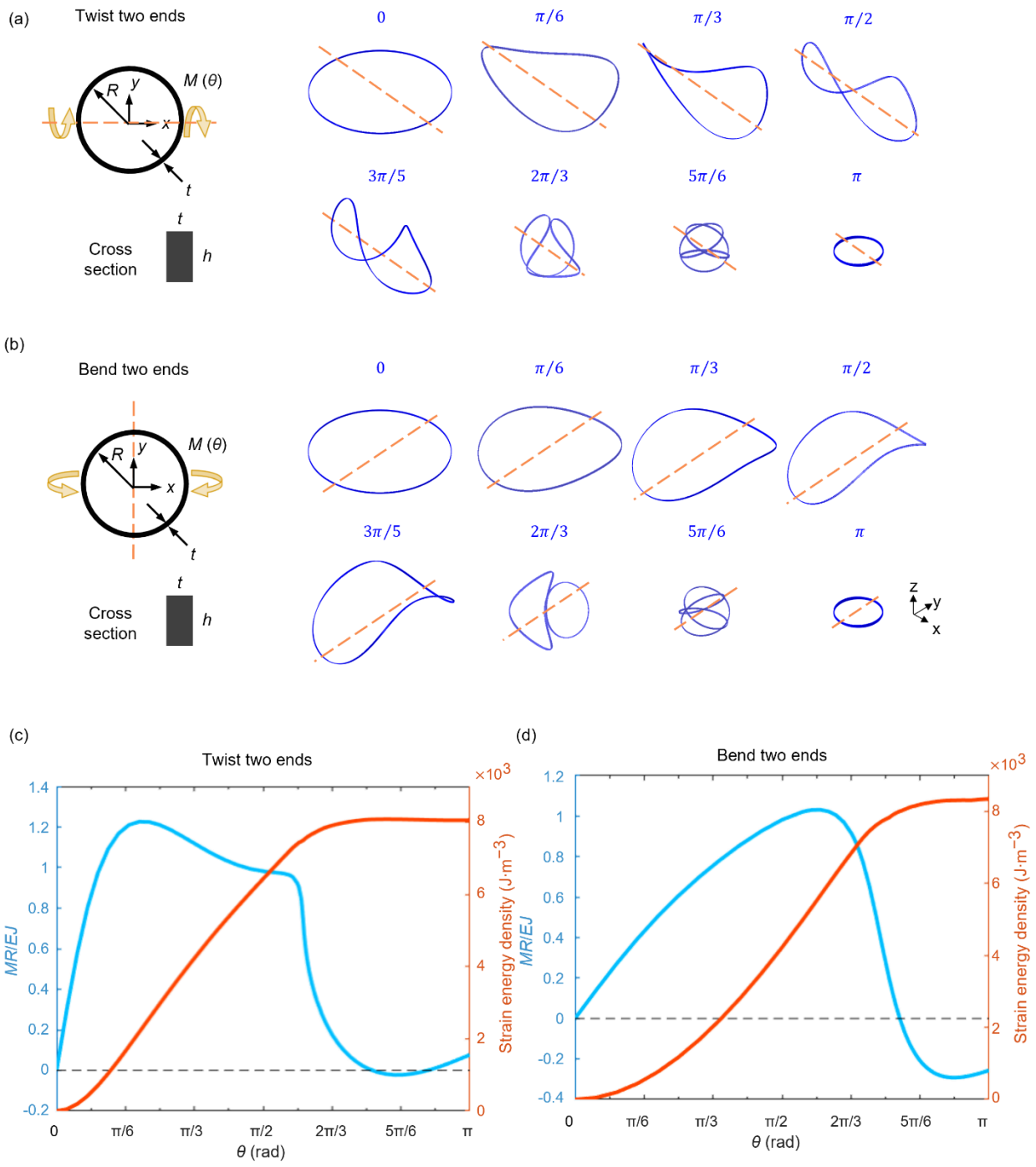

Figure S1. Twisting and bending of circular rings. (a) Twisting-induced snap-folding. (b) Bending-induced snap-folding. (c) The moment-twisting angle curve and strain energy density curve for twisting. (d) The moment-bending angle curve and strain energy density curve for bending.

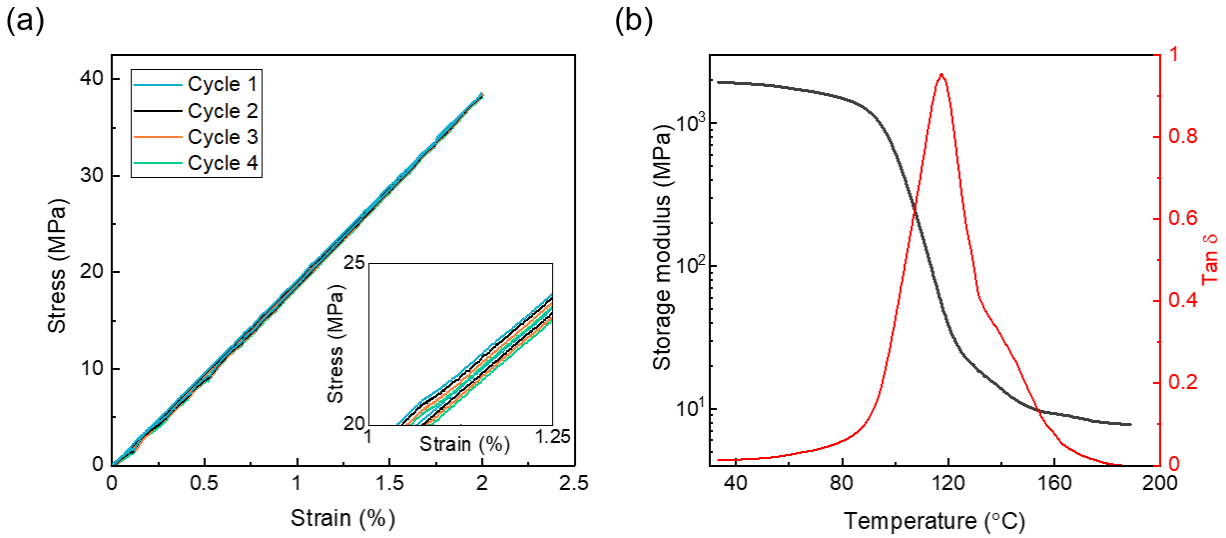

Figure S2. Mechanical characterization of material used for ring fabrication. (a) Stress-strain curves of the cured resin under cyclic loading-unloading. Linear curve fitting of 1% strain indicates a Young's modulus of 1.8 GPa. (b) DMA measurement of the cured resin shows a glass transition temperature of 118℃.

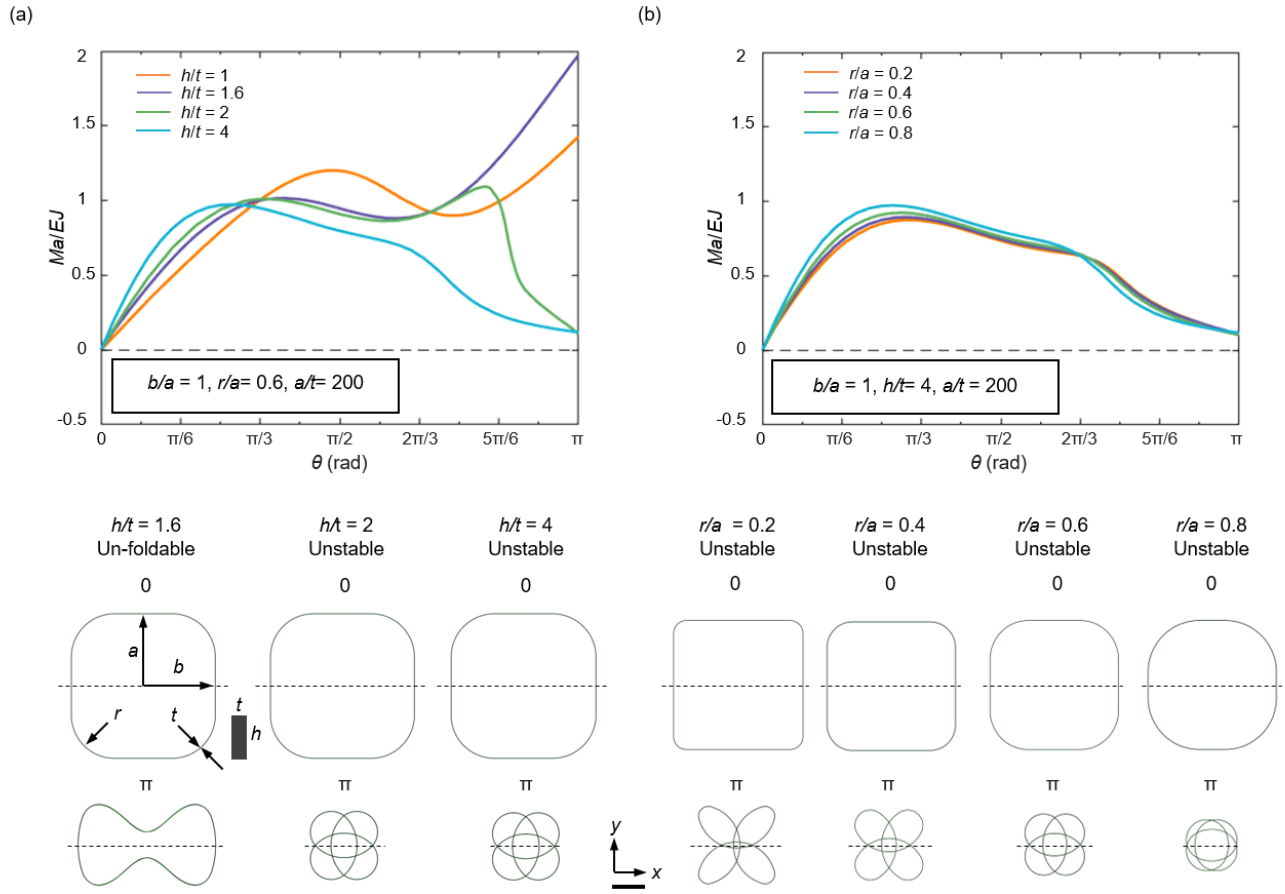

Figure S3. Parametric study of the rounded rectangular rings for $b/a = 1$. The effect of geometric parameters (a) h/t and (b) r/a on snap-folding of rounded rectangular rings. Scale bar: 5mm.

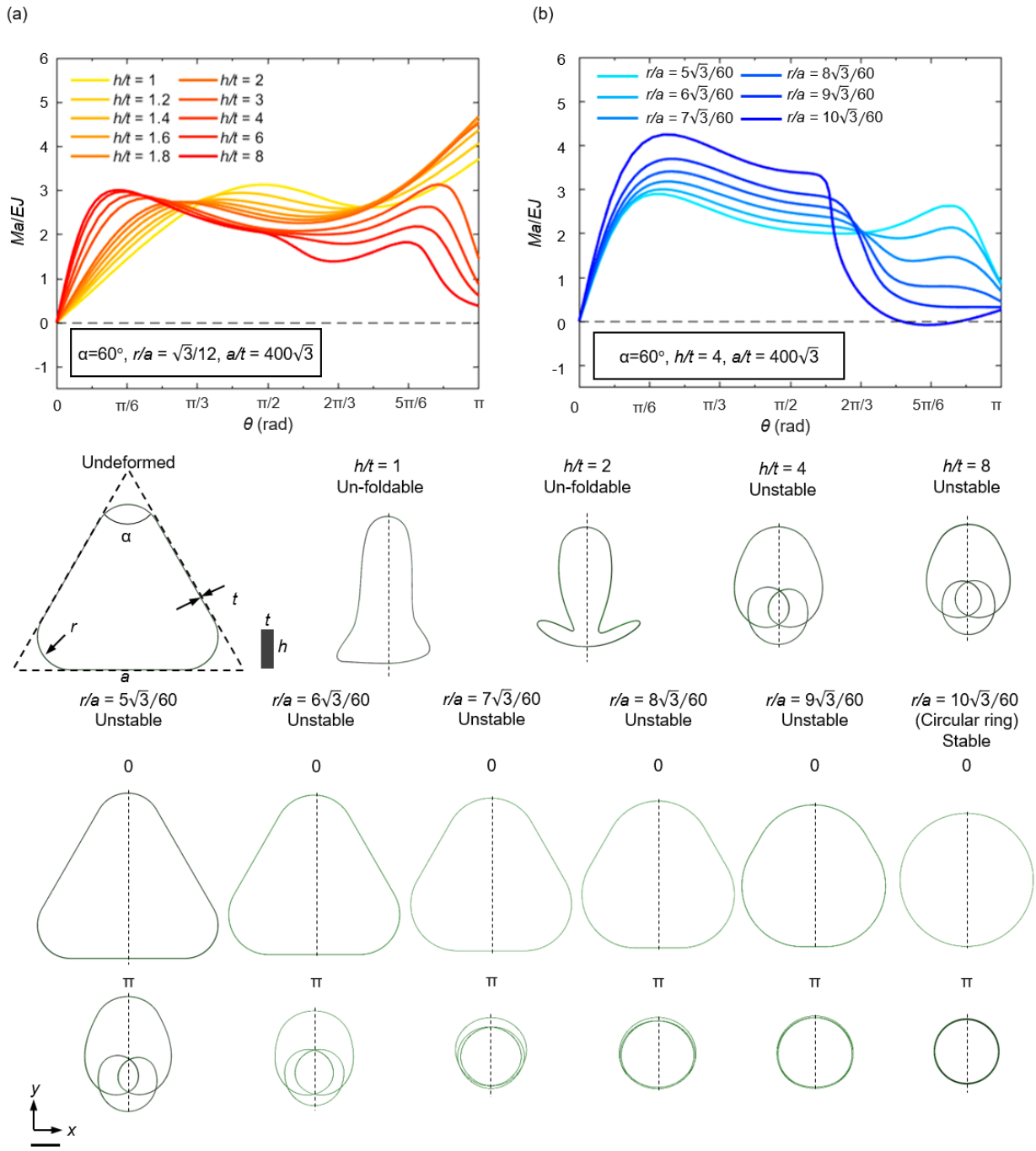

Figure S4. Parametric study of the triangular rings for $\alpha = 60°$. The effect of geometric parameters (a) *h/t* and (b) *r/a* on snap-folding of triangular rings. Scale bar: 5mm.

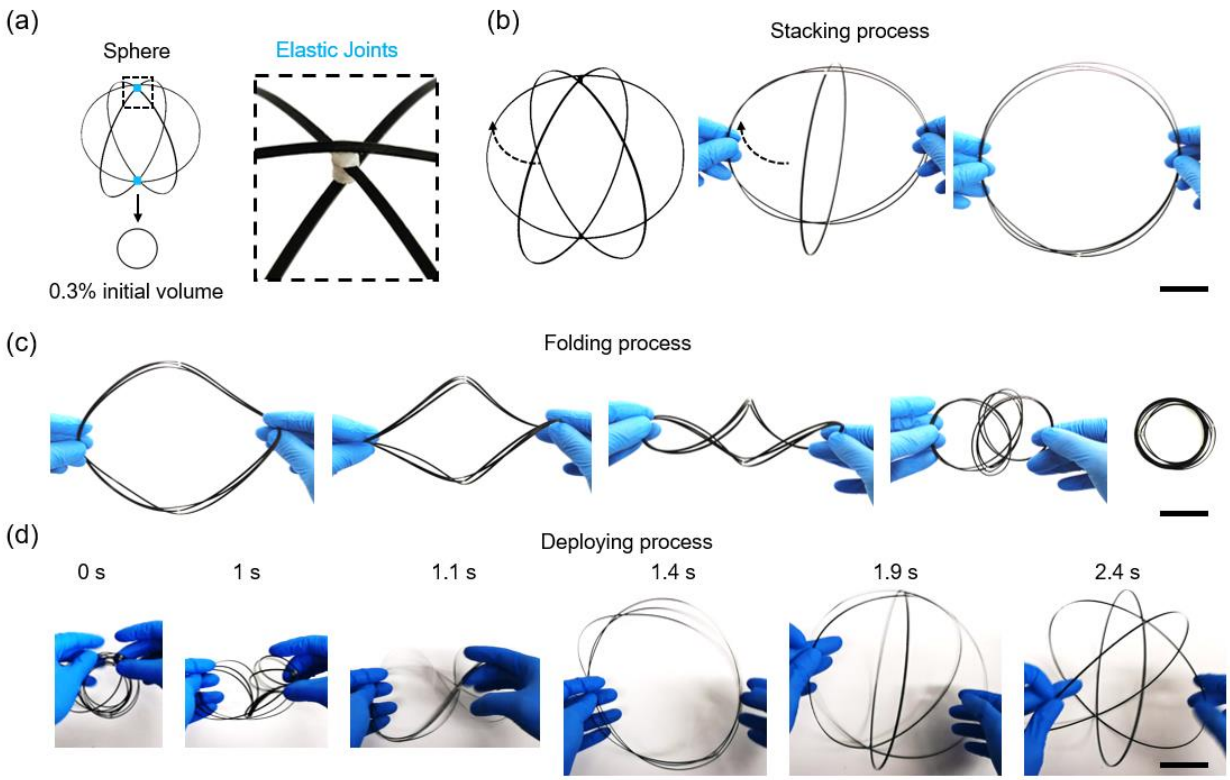

Figure S5. Stacking, snap-folding and snap-deploying of a 3D ring sphere made of three crossing circular rings. (a) Three circular rings connected by cylindrical silicone rubber joints. (b) Stacking process. (c) Snap-folding process. (d) Snap-deploying process. Scale bars: 5cm.

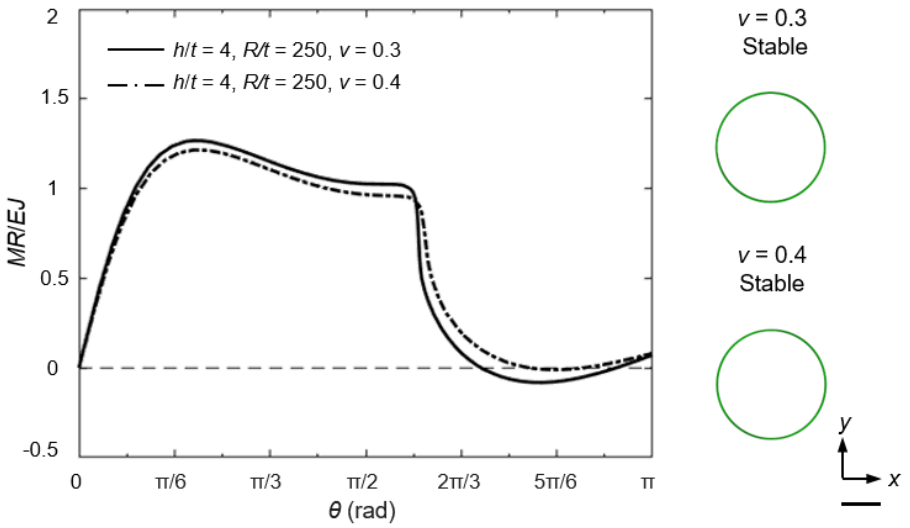

Figure S6. Effect of Poisson's ratio (v) on snap-folding of circular rings. Scale bar: 7 mm.

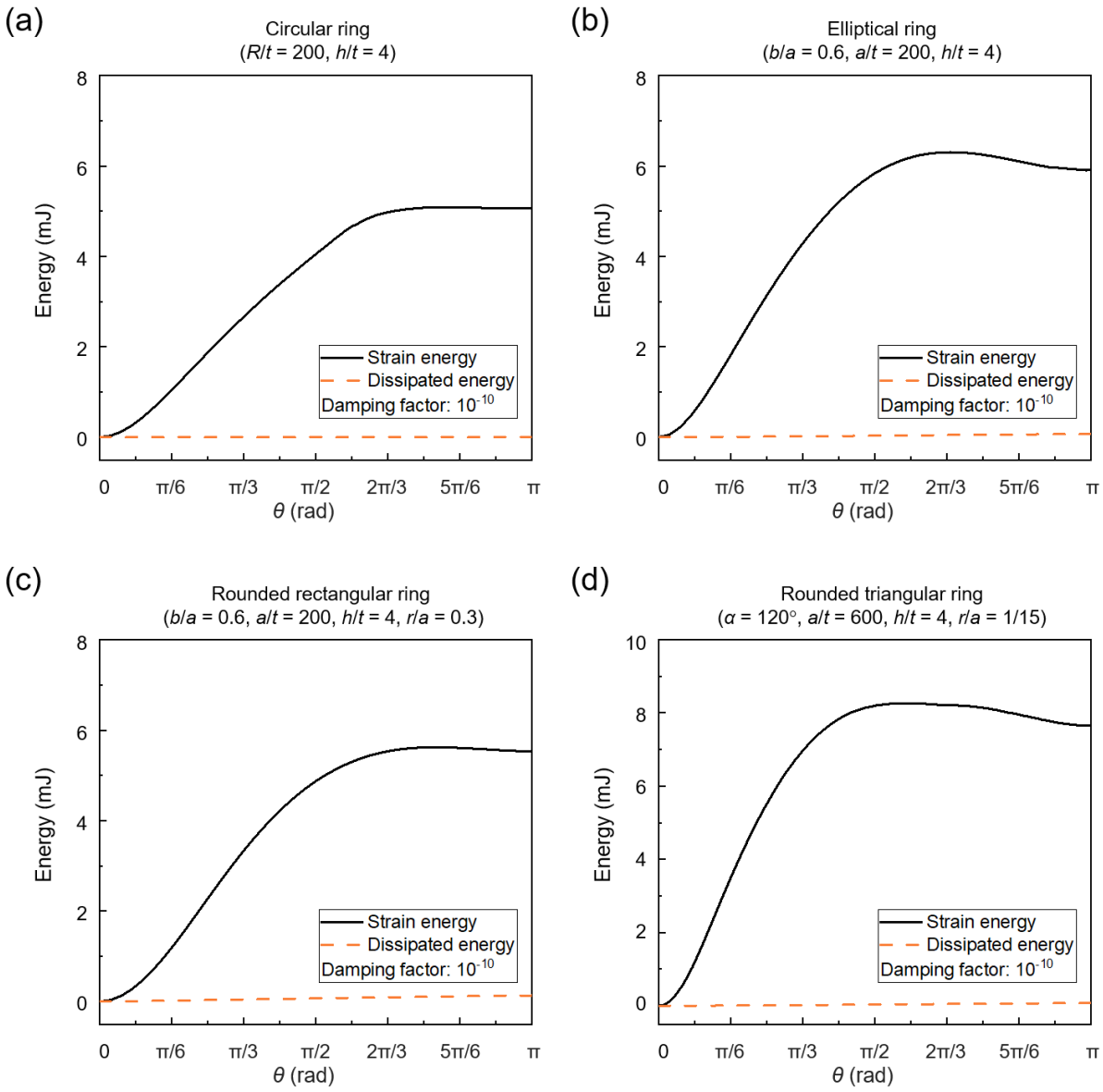

Figure S7. Strain energy and dissipated energy of (a) circular ring, (b) elliptical ring, (c) rounded rectangular ring, and (d) rounded triangular ring during folding.